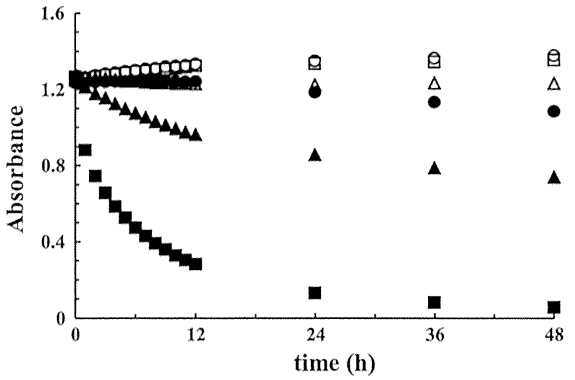

Fig. 5 Plots of absorbance at λ_{max} of the $CHCl_3$ solutions of compound **8e** (λ_{max} = 678 nm) under illumination (*solid circles*) and in dark (*open circles*), compound **3** (λ_{max} = 676 nm) under illumination (*solid triangle*) and in dark (*open triangles*), and Zn*t*BPc (λ_{max} = 678 nm) under illumination (*solid squares*) and in dark (*open squares*)

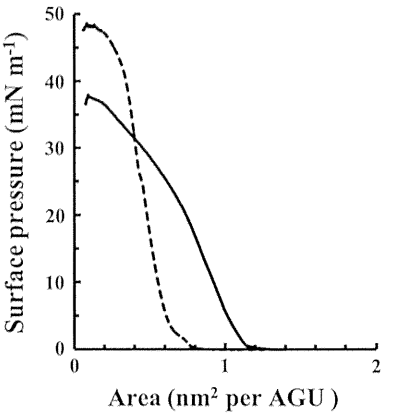

Fig. 6 Surface pressure (π)–area (A) isotherms of compound **8e** (*solid line*) and compound **1** (*dotted line*)

compound **8e**, and Zn*t*BPc were stored in the dark, the absorption properties of both solutions remained almost the same, even after 48 h. Following 48 h under the illumination conditions, however, the absorption of the Zn*t*BPc solution was reduced from 1.27 to 0.06 (rate of decline: 95 %). The absorptions at 612 and 348 nm were also reduced significantly (Fig. S2c in supporting information). In contrast, the absorption of the compound **8e** solution was only reduced from 1.23 to 1.08 (rate of decline: 12 %). The other bands also behaved in a similar manner (Fig. S2a in Supporting Information). The absorption at 676 nm of compound **3** solution was reduced from 1.26 to 0.74 (rate of decline: 41 %) and the other bands also decayed (Fig. S2b in supporting information). The rates of decline of Q bands and Soret bands of phthalocyanine in the cellulose derivatives **8e** and **3** solutions were much smaller than those of Zn*t*BPc solution, suggesting that the cellulose backbone was contributing to the photostability of the phthalocyanine moieties in compound **8e**. Furthermore, the photostability of phthalocyanine moieties in compound **8e** was improved from that in compound **3** although further investigation for understanding the mechanism for the photostability is required.

Preparation of LB monolayer films of cellulose derivative 8e

Figure 6 shows the surface pressure (π)–area (A) isotherms of compounds **8e** and **1** at the air–water interface at 20 °C. The limiting molecular areas of compounds **8e** and **1** were 1.11 and 0.602 nm^2 per anhydroglucose unit (AGU), respectively. These values were obtained from the extrapolation of the steepest part of the isotherm to zero surface pressure. Because compounds **8e** and **1** can be considered as cellulose derivatives with and without the phthalocyanine moieties, respectively, the limiting molecular area of the phthalocyanine moieties of compound **8e** was calculated to 0.508 nm^2 when the phthalocyanine units were assumed to have no influence on the arrangement of the cellulose backbone. Matsuura et al. (2000) estimated the limiting molecular area of tetrakis(*tert*-butyl)phthalocyanine to be approximately 0.60 nm^2 on the basis that the phthalocyanine rings were perpendicular to the surface of the water. With this in mind, it was suggested that the phthalocyanine units of compound **8e** were oriented almost perpendicular to the surface of the water.

In a recently published paper (Saito et al. 2012), LB monolayer films of compound **3** were successfully deposited on a series of different substrates at a surface pressure of 10 mN/m using the vertical dipping method. Interestingly, the total area of the monolayer of compound **3** decreased gradually when the surface pressure was maintained at 10 mN/m. The annealing time (maintaining a constant surface pressure until the deposition process) was determined to be one of the most important factors for obtaining homogeneous LB monolayer films, with 90 min found to be the optimum time for the construction of LB monolayers of compound **3**. In the current paper, LB monolayer

Table 3 Preparation of LB monolayer films of compound **8e**

Film	Transfer method	Substrate	Annealing time[a] (min)	Transfer ratio	
				down	up
A	Vertical dipping	Quartz	5	0.09	1.00
A′	Vertical dipping	Mica	5	0.00	1.15
A″	Vertical dipping	ITO electrode	5	0.13	1.02
B	Vertical dipping	Quartz	10	0.10	1.01
C	Vertical dipping	Quartz	30	0.09	1.11
D	Horizontal lifting	Quartz	5	–	–

[a] Keeping time at the constant surface pressure (10 mN/m) till deposition

films of compound **8e** were prepared on quartz using the vertical dipping method and a variety of different annealing times, including 5, 10, and 30 min (films A-C, respectively) (Table 3). The monolayers of compound **8e** were transferred only partially by the first downward stroke, and then thoroughly by the upward stroke. The transfer ratios of the latter were almost 1.0. Figure 7a shows the UV–vis spectra of the LB monolayer films A–C. The representative bands from the phthalocyanine moieties, especially the Q bands, were significantly reduced in the spectra of films B and C, whereas they were still clearly present in the spectrum of film A. The results of these experiments suggested that application of a long annealing time was not suitable for the preparation of LB monolayer films of compound **8e**, contrary to the report concerning the formation of LB monolayers of compound **3**. It might be that the rate of arrangement of compound **8e** at the air/water interface was faster than that of compound **3** because compound **8e** contained only phthalocyanine moieties at *O*-6 position whereas compound **3** contained not only phthalocyanine moieties but also unreacted dicyanophenyl groups and groups derived from the dicyanophenyl groups that had reacted with *O*-phthalodinitriles but did not form phthalocyanin-ring. An LB monolayer film of compound **8e** (film D) was also prepared using the horizontal lifting method with an annealing time of 5 min. The characteristic bands of the phthalocyanine moieties, however, were only barely visible. LB monolayer films of compound **8e** were also prepared on a variety of different substrates (films A: on quartz, A′: on mica, A″: on an indium tin oxide (ITO) electrode) using the vertical dipping method with an annealing time of 5 min (Table 3), and subjected to the characterization and evaluation processes described below.

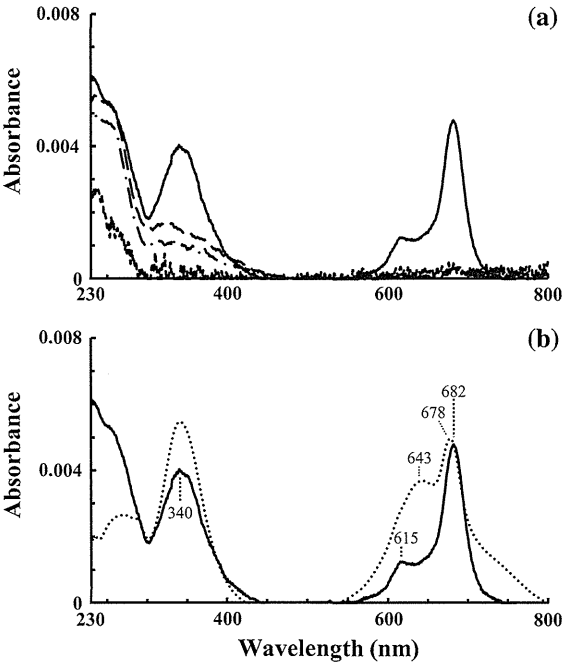

Fig. 7 UV–vis spectra of LB monolayer films A (*solid line*), B (*long dashed line*), C (*long dashed dotted line*), and D (*dotted line*) of compound **8e**: (**a**), UV–vis spectra of LB monolayer film A (*solid line*) and the $CHCl_3$ solution (*dotted line*) of compound **8e** (normalized at 682 nm) : (**b**)

Characterization of the LB monolayer films of cellulose derivative **8e**

Figure 7b shows the UV–vis spectra of the LB monolayer film A of compound **8e** on quartz (solid state) and the chloroform solution of compound **8e** (solution state). The latter is the same spectrum in Fig. 4a. The strong and weak bands at 682 and 615 nm, respectively, in the Q bands were present in the spectrum of film A, whereas the strong bands at 678 and 643 nm were present in the spectrum of the

solution. There are two important points to be discussed with regard to the differences between these spectra. The first of these points pertains to the band at 643 nm, which is known to be derived from the Q bands of a dimeric complex formed from the phthalocyanine units (Allcock and Neenan 1986). The intensity of this band was reduced in the spectrum of film A, suggesting that the cellulose backbone effectively suppressed the aggregation of the phthalocyanine moieties as a scaffold in film A. The second point pertains to the maximum band in the Q bands of compound **8e,** which was red-shifted from 678 nm in the solution to 682 nm in film A. Qiu et al. (2008) reported that the red- and blue-shifts of the Q bands of zinc phthalocyanine that were caused by the chromophoric packing corresponded to the edge-to-edge packing (*J*-aggregates) and face-to-face packing (*H*-aggregates) properties, respectively. The packing of phthalocyanine moieties in film A could be *J*-aggregates. To confirm the type of packaging within the films, film A was subjected to polarized UV–vis measurements. The tilt angle θ, which refers to the angle between the phthalocyanine plane and the substrate plane was calculated for film A from the maximum absorbance of the Q band in the polarized UV–vis spectra of film A with different incident angles (Fig. S3 of the Supporting Information), according to the method reported by Yoneyama et al. (1986). The tilt angle was estimated to be 23.7°. Since packing with a tilt angle in the range of 0–54.7° is defined as *J*-aggregate packing (Qiu et al. 2008), the current result indicated that a *J*-aggregated stacked structure of the phthalocyanine moieties of compound **8e** had formed along the cellulose backbone of the LB monolayer film A. In other words, the phthalocyanine moieties were densely packed in the LB monolayer film A.

The LB monolayer film of compound **8e** on mica (film A′; transfer ratio: downward stroke: 0.00, upward stroke: 1.15) was analyzed by AFM. The AFM image of film A′ is shown in Fig. 8. Several aggregates and holes were observed on the image of film A′, suggesting that LB monolayer film A′ was not homogeneous, although it was suggested from the UV–vis spectrum of film A (Fig. 7b) that the aggregation of the phthalocyanine moieties of film A was suppressed.

The photocurrent density (photocurrent per unit area of a working electrode) of the LB monolayer of compound **8e** on an ITO electrode (film A″; transfer ratio: downward stroke: 0.13, upward stroke: 1.02) was evaluated as photocurrent generation performance. Figure 9 shows the action spectrum of film A″ (closed circle) as well as the UV–vis spectrum of film A. The previously reported action spectrum of the LB monolayer film of compound **3** (open circle) is also shown in Fig. 9. The pattern of the action spectrum of film A″ was similar to that observed for the UV–vis spectrum of film A in the region of 600–700 nm. This result suggested that the phthalocyanine moieties were effectively behaving as photoactive species for the generation of the photocurrent in that region. This suggestion was confirmed by the photocurrent values

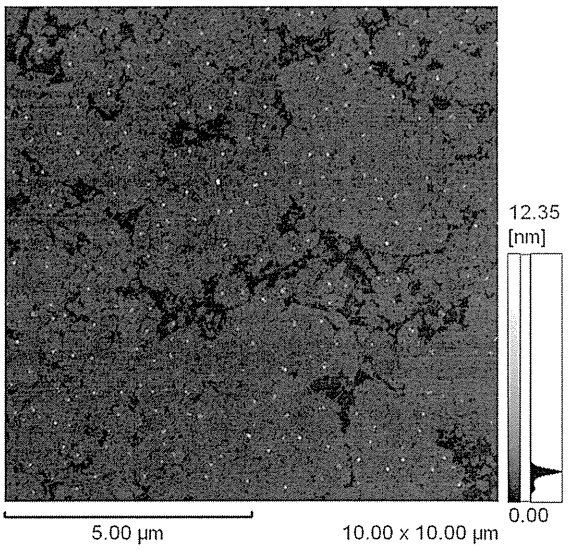

Fig. 8 AFM image of the LB monolayer film A′ of compound **8e** deposited on freshly cleaved mica at a surface pressure of 10 mN/m at 20 °C

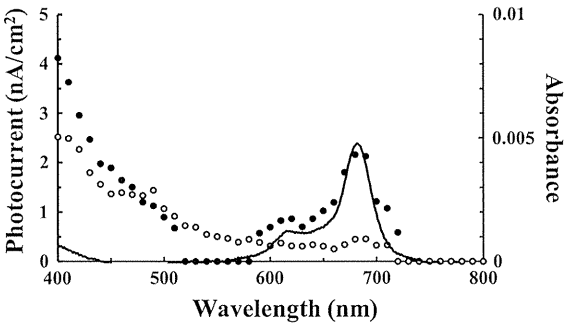

Fig. 9 Action spectra of the LB monolayer film A″ of compound **8e** (*closed circle*) and of compound **3** (*open circle*). *Solid line* shows UV–vis spectrum of LB monolayer film A of compound **8e**

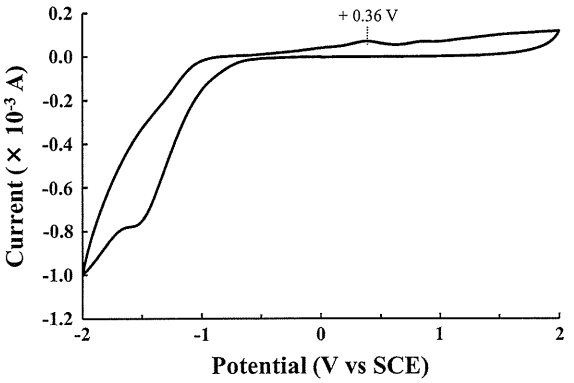

Fig. 10 Cyclic voltommogram of LB monolayer film A″ of compound **8e** in acetonitrile solution containing 0.1 M $(n\text{-Bu})_4NPF_6$ as supporting electrolyte. Scan rate: 100 mV/s

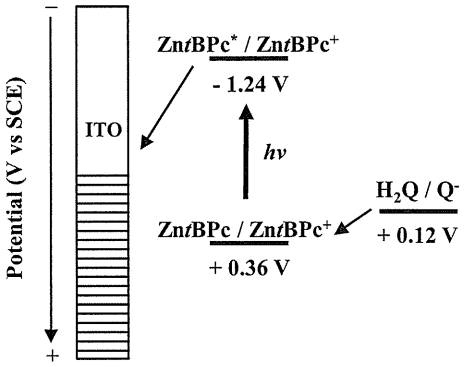

Fig. 11 Energy diagram of the present evaluation system (H_2Q hydroquinone, Q^- semiquinone)

for film A″ which were higher than those of the film constructed from compound **3**. In other words, the photocurrent density for the film composed of compound **3** at 680 nm (0.45 nA/cm^2) was improved relative to that of film A″ (2.16 nA/cm^2), although the performance of this material remained far from satisfactory.

One of the reasons for unsatisfactory photocurrent performance of film A″ could be related to the unsuitable energy diagram of the evaluation system, because the system was established for a LB film of porphyirn-containing cellulose derivatives (Sakakibara et al. 2007). To reconfirm the suitability of the energy diagram of the system for films composed of phthalocyanine-bearing cellulose derivatives, film A″ was analyzed by CV. The CV curve of film A″ was in good agreement with that of the LB monolayer film reported by Yang et al. (2003) for [2,3,9,10,16,17,23,24-octakis(octyloxy)phthalocyaninato]zinc(II), and the first oxidation peak of film A″ was clearly present at 0.36 V versus the saturated calomel electrode (SCE) (Fig. 10). On the basis of data from the literature data, including the HOMO–LUMO energy gap of zinc phthalocyanine, which was reported to be 1.60 eV by Yang et al. (2003), and the oxidation potential of hydroquinone, which was reported to be 0.12 V (vs. SCE) by Sereno et al. (1996), we were able to construct an energy diagram for the system as shown in Fig. 11. This diagram was found to be satisfactory for the evaluation of the photocurrent of LB films of phtalocyanine-containing cellulose derivatives.

Conclusion

2,3-Di-*O*-myristyl-6-*O*-[*p*-(9(10),16(17),23(24)-tri-*tert*-butyl-2-phthalocyaninyl)-benzoyl] cellulose (**8e**) with a $DS_{phthalocyanine}$ of 0.33 has been synthesized in a high yield via the esterification of Zn*t*BPc-COOH (**7**) with 2,3-di-*O*-myristyl cellulose (**1**), although the preparation Zn*t*BPc-COOH (**7**) was time consuming and laborious. A chloroform solution of compound **8e** was found to be more stable under illumination than that of Zn*t*BPC. The LB monolayer films of compound **8e** on a variety of different substrates were constructed using the vertical dipping method with an annealing time of 5 min. The results of the current study revealed that *J*-aggregated stacked structures of the phthalocyanine moieties of compound **8e** had formed along the cellulose backbone in the LB monolayer film. The LB monolayer film of **8e** on an ITO electrode showed photocurrent generation properties in the range of 600–700 nm, which corresponded to the Q bands of the phthalocyanine moieties as expected. The photocurrent generation performance of the LB monolayer film of compound **8e** was greater than that of compound **3**, although it was not still satisfactory. To enable further improvements in the photocurrent generation properties of the LB monolayer films constructed from compound **8e**, we are currently investigating changes to the chemical structure of the phthalocyanine-containing cellulose derivatives with the aim of enhancing the homogeneity of these materials during the preparation of the LB films.

References

Allcock HR, Neenan TX (1986) Synthesis of polyphosphazenes bearing covalently linked copper phthalocyanine units. Macromolecules 19(6):1495–1501. doi:10.1021/ma00160a001

Burke A, Schmidt-Mende L, Ito S, Grätzel M (2007) A novel blue dye for near-IR 'dye-sensitized' solar cell applications. Chem Commun: 234–236. doi:10.1039/b609266g

Choudhury B, Weedon AC, Bolton JR (1998) Effects of molecular organization on photophysical behavior. 2. Photoelectrochemical and photocurrent quantum yield studies of the Langmuir–Blodgett monolayers of some surfactant porphyrins. Langmuir 14:6199–6206. doi:10.1021/la971338i

Cid J-J, García-Iglesias M, Yum J-H, Forneli A, Albero J, Martínez-Ferrero E, Vázquez P, Grätzel M, Nazeeruddin MK, Palomares E, Torres T (2009) Structure–function relationships in unsymmetrical zinc phthalocyanines for dye-sensitized solar cells. Chem Eur J 15(20):5130–5137. doi:10.1002/chem.200801778

Erdem SS, Nesterova IV, Soper SA, Hammer RP (2008) Solid-phase synthesis of asymmetrically substituted "AB_3-Type" phthalocyanines. J Org Chem 73(13):5003–5007. doi:10.1021/jo800536v

Imahori H, Hozomizu K, Mori Y, Sato T, Ahn TK, Kim SK, Kim D, Nishimura Y, Yamazaki I, Ishii H, Hotta H, Matano Y (2004) Substituent effects of porphyrin monolayers on the structure and photoelectrochemical properties of self-assembled monolayers of porphyrin on Indium-tin oxide electrode. J Phys Chem B 108(16):5018–5025. doi:10.1021/jp037625e

Isago H, Miura K, Kanesato M (2008) Unexpected photo-initiated oxidation of antimony in (tetra-*tert*-butyl)phthalocyaninatoantimony(III) complex in the presence of singlet oxygen acceptors. J Photoch Photobio A 197(2–3):313–320. doi:10.1016/j.jphotochem.2008.01.009

Matsuura T, Komatsu T, Hatta E, Shimoyama Y (2000) Enhanced orientation in Langmuir–Blodgett films of tetra-*tert*-butyl phthalocyanines. Jpn J Appl Phys 39(4A):1821–1825. doi:10.1143/JJAP.39.1821

Mori S, Nagata M, Nakahata Y, Yasuta K, Goto R, Kimura M, Taya M (2010) Enhancement of incident photon-to-current conversion efficiency for phthalocyanine-sensitized solar cells by 3D molecular structuralization. J Am Chem Soc 132(12):4054–4055. doi:10.1021/ja9109677

Qiu Y, Chen P, Liu M (2008) Interfacial assembly of an achiral zinc phthalocyanine at the air/water interface: a surface pressure dependent aggregation and supermolecular chirality. Langmuir 24:7200–7207. doi:10.1021/la703703e

Redl FX, Lutz M, Daub J (2001) Chemistry of porphyrin-appended cellulose strands with a helical structure: spectroscopy, electrochemistry, and in situ circular dichroism spectroelectrochemistry. Chem Eur J 7(24):5350–5358

Saito Y, Takano T, Sakakibara K, Kamitakahara H, Nakatsubo F (2012) Synthesis of (zinc(II) phthalocyanine)-containing cellulose derivative using phthalocyanine-ring formation reaction. Cellulose 19(6):2105–2114. doi:10.1007/s10570-012-9772-7

Sakakibara K, Nakatsubo F (2008) Effect of fullerene on photocurrent performance of 6-*O*-porphyrin-2,3-di-*O*-stearoylcellulose Langmuir–Blodgett films. Macromol Chem Phys 209(12):1274–1281. doi:10.1002/macp.200800027

Sakakibara K, Nakatsubo F (2010) Effect of central metals in the porphyrin ring on photocurrent performance of cellulose Langmuir–Blodgett films. Macromol Chem Phys 211(22):2425–2433. doi:10.1002/macp.201000257

Sakakibara K, Ogawa Y, Nakatsubo F (2007) First cellulose Langmuir–Blodgett films towards photocurrent generation systems. Macromol Rapid Commun 28(11):1270–1275. doi:10.1002/marc.200700130

Sereno L, Silber JJ, Otero L, Bohorquez MDV, Moore AL, Moore TA, Gust D (1996) Photoelectochemistry of Langmuir–Blodgett films of carotenoid pigments on ITO electrodes. J Phys Chem 100(2):814–821. doi:10.1021/jp952300m

Shirai H, Hanabusa K, Kitamura M, Masuda E, Hirabaru O, Hojo N (1984) Functional metal porphyrazine derivatives and their polymers, 14: synthesis and properties of [bis- or tetrakis(decyloxycarbonyl)phthalocyaninato]metal complexes. Makromol Chem 185:2537–2542

Sobbi AK, Wöhrle D, Schlettwein D (1993) Photochemical stability of various porphyrins in solution and as thin film electrodes. J Chem Soc Perkin Trans 2:481–488. doi:10.1039/P29930000481

Stota R, Dyrda G (2003) UV photostability of metal phthalocyanines in organic solvents. Inorg Chem 42(18):5743–5750. doi:10.1021/ic0260217

Yang S, Fan L, Yang S (2003) Preparation, characterization, and photoelectrochemistry of Langmuir–Blodgett films of the endohedral metallofullerene $Dy@C_{82}$ mixed with metallophthalocyanines. J Phys Chem B 107(33):8403–8411. doi:10.1021/jp035107y

Yoneyama M, Sugi M, Saito M, Ikegami K, Kuroda S, Iizima S (1986) Photoelectric properties of copper phthalocyanine Langmuir–Blodgett film. Jan J Appl Phys 25(7):961–965

Journal of Wood Chemistry and Technology, 34:262–272, 2014

ISSN: 0277-3813 print / 1532-2319 online
DOI: 10.1080/02773813.2013.869605

Taylor & Francis
Taylor & Francis Group

Preparation and Evaluation of the Oxidation Ability of Hematin-Appended 6-Amino-6-Deoxycellulose

MAKI OZAWA, ASUKA FUKUTOME, YUMI SANNAMI, HIROSHI KAMITAKAHARA, AND TOSHIYUKI TAKANO

Division of Forest and Biomaterials Science, Graduate School of Agriculture, Kyoto University, Kyoto, Japan

Abstract: *The reaction of 6-amino-6-deoxycelluloe (**1**) with hematin in the presence of* N,N′*-carbonyldiimidazole and 1,8-diazabicyclo[5.4.0]undec-7-ene in* N,N*-dimethylformamide at 50°C for four days afforded hematin-appended 6-aminocellulose (**2**). Compound **2** was more stable than hematin, and retained the oxidation activity of hematin, even after being treated at 100°C for 3 h. Compound **2** showed good guaiacol oxidation activity in an aqueous 80% AcOH solution (pH 1.5), whereas hematin and horseradish peroxidase showed very low oxidation activities under the same conditions, suggesting that compound **2** is a useful biomimetic catalyst. However, no asymmetric induction was achieved in the catalytic oxidation of sinapyl alcohol (**3**) using compound **2**.*

Keywords Biomimetic catalyst, cellulose derivative ferriprotoporphyrin, porphyrin, sinapyl alcohol

Introduction

Porphyrin-containing cellulose materials are representative of several recent proposals for the high-value-added utilization of cellulose, with examples reported in the literature, including 6-*O*-porphyrinyl cellulose derivatives for electrochromism-based switching materials,[1] hematoporphyrin immobilized cellulose microfibers for oxygen sensors,[2] 6-*O*-porphyniyl cellulose derivatives for photocurrent generation systems,[3] and porphyrin (Hemin)-grafting cellulose nanometric films for the protection of inorganic materials.[4]

Hematin is a hydroxy ferriprotoporphyrin with a structure similar to that of the prosthetic iron protoporphyrin IX in horseradish peroxidase (HRP), which is a well-known enzyme for the oxidation of phenols, and is expected to become an alternative biomimetic catalyst to HRP.[5,6] Unfortunately, however, there are several disadvantages associated with hematin, including low oxidation activity because of self-aggregation in solution, and low solubility in acidic (low pH) solutions. Polyethylene glycol (PEG)-supported hematin has been reported to improve the solubility and self-aggregation properties of hematin.[7,8] In contrast, 6-amino-6-deoxycellulose (**1**) has been suggested as a promising scaffold for

Address correspondence to Toshiyuki Takano, Division of Forest & Biomaterials Science, Graduate School of Agriculture, Kyoto University, Sakyo-ku, Kyoto 606-8502, Japan. E-mail: takatmys@kais.kyoto-u.ac.jp

Color versions of one or more of the figures in the article can be found online at www.tandfonline.com/lwct.

hematin because it possesses a regular structure and is soluble in acidic aqueous solutions. Furthermore, this material is a chiral polymer, and an asymmetric synthesis involving a chiral water-soluble iron porphyrin has recently been reported in the literature.[9] Hematin-appended 6-amino-6-deoxycellulose (6-ADC/Hem) (**2**) has also been identified as an attractive new biomimetic catalyst. It has also been interesting as an oxidation catalyst for the polymerization of monolignol to investigate the influence of cellulose to lignin structure. To the best of our knowledge, there has only been one report in the literature to date concerning a hematin-containing polysaccharide, which was a hematin-containing agarose.[10] The focus of this particular report, however, was limited to affinity chromatography. In the current article, we have therefore described the preparation and evaluation of the oxidation activity of 6-ADC/Hem (**2**).

Materials and Methods

Materials

6-Amino-6-deoxycellulose (**1**) with a DS_{NH2} value of 0.90 was prepared according to the method previously described by Matsui et al.[11] Hematin and HRP (100 U mg^{-1}) were purchased from Sigma-Aldrich (Tokyo, Japan) and Wako Chemical Co. (Osaka, Japan), respectively. (+)-Syringaresinol and (−)-syringaresinol were prepared by enzymatic hydrolysis of (±)-syringaresinol di-β-D-glucopyranoside[12] with cellulase (Wako). All of the other chemicals used in the current study were purchased from commercial sources and used without further purification.

Measurements

Fourier transform infrared (FT-IR) spectra were recorded as KBr pellets on a Shimadzu FTIR-8600 spectrophotometer (Shimadzu, Kyoto, Japan). ^{1}H-NMR spectra were recorded on a Varian500 FT-NMR (500 MHz) spectrometer (Agilent Technologies, Santa Clara, CA, USA) with tetramethylsilane used as an internal standard in a 4:1 (v/v) mixture of CD_3COOD/D_2O. Chemical shifts (δ) have been reported in δ values (ppm). UV-Vis spectra were recorded on a Jasco V-560 UV-vis spectrophotometer (Jasco, Tokyo, Japan). High-performance liquid chromatography (HPLC) analyses were performed on a Shimadzu LC-10 system equipped with a Shimadzu UV-Vis detector (SPD-10Avp) (Shimadzu) and a CHIRALCEL OD-3 column (Daicel, Osaka, Japan). CH_3OH was used an eluent with a flow rate of 0.5 mL min^{-1}. The cyclic voltammetry (CV) measurements were performed with an ALS electrochemical analyzer (ALS 650B, BAS, Tokyo, Japan) in an undivided cell (5 mL) [working electrode: 1.6 mm diameter platinum disk, reference electrode: Ag/Ag+ reference electrode, counter electrode: platinum wire, electrolyte: 5 mM sodium acetate in an aqueous 80% AcOH solution].

Preparation of Hematin-Appended 6-Amino-6-Deoxycellulose (6-ADC/Hem) (2)

N,N′-Carbonyldiimidazole (CDI) (101 mg, 0.62 mmol) and 1,8-diazabicyclo[5,4,0]undec-7-ene (DBU) (92.7 μL, 0.62 mmol) were added sequentially to a stirred solution of hematin (393.2 mg, 0.62 mmol) in *N,N*-dimethylformamide (DMF) (10 mL) at room temperature under an atmosphere of nitrogen, and the resulting solution was stirred at room temperature for 30 min. 6-Amino-6-deoxycellulose (**1**) powder (100 mg, 0.62 mmol) was then added to

the solution, and the resulting suspension was stirred at 50°C for four days. The mixture was then cooled to ambient temperature and filtered. The filter-cake was washed 10 times with DMF before being collected to afford the crude product, which was stirred in DMF (300 mL) at room temperature for 24 h. The mixture was then filtered and the filter-cake was washed three times with MeOH before being dried under vacuum to give compound **2** (88.3 mg). FT-IR (KBr): ν 3350, 2916, 1709, 1643, 1568, 1385, 1069, 937, 839, 718 cm^{-1}; ^1H NMR (CD_3COOD/D_2O = 4/1 (v/v)): δ 8.80, 8.20, 7.53 (Hematin-H), 5.0–3.0 (AGU-H) ppm.

Stability Testing of 6-ADC/Hem (2) in an Aqueous 80% AcOH Solution

An aqueous 80% AcOH solution (0.01 mg mL^{-1}) of compound **2** with its maximum absorbance at the Soret band of 0.496 was prepared and subjected to UV-Vis measurements within 30 minutes of its preparation. Following the measurements, half of the solution was heated at 100°C for 3 h, whereas the other half was kept at ambient temperature for three days. The solutions were then subjected to UV-Vis measurements. An aqueous 80% AcOH solution of hematin (concentration: 2.76 μg/mL) was also prepared with the same maximum absorbance at the Soret band (0.497) and tested in the same manner as the reference material.

The aqueous 80% AcOH solutions of compound **2** and hematin described above were prepared a second time in the same way and subjected to UV-Vis measurements over a 25-min period at 5 min intervals following the addition of an 18 mM aqueous H_2O_2 solution (50 μL, 0.9 μmol).

Guaiacol Oxidation Activity Assay of 6-ADC/Hem (2) in an Aqueous 80% AcOH Solution

An aqueous 80% AcOH solution of compound **2** was prepared and divided between the sample and reference cells, with the amount of compound **2** in each cell being set at 0.03 mg. Guaiacol (9.0 μmol) was added to the solutions in the sample cells, and the cells were then placed in the UV-Vis spectrophotometer. Following the addition of a 180 mM aqueous H_2O_2 solution (50 μL, 9.0 μmol) to each of the sample cells, the cells were kept at 25°C under stirring, and their absorbance at 470 nm, which was derived from the guaiacol oxidation products, was monitored. The solutions of hematin, HRP, and compound **2** that had been subjected to the different treatments described above (i.e., ambient temperature for three days or 100°C for 3 h) with the same maximum absorbance at the Soret band in an aqueous 80% AcOH solution were prepared and tested in the same manner. A guaiacol oxidation assay of compound **2** was also performed with different concentrations of H_2O_2 (the amounts of H_2O_2 in the sample cells were 0.9, 1.8, 9.0, and 18.0 μmol).

6-ADC/Hem (2)-Catalyzed Oxidation of Sinapyl Alcohol in an Aqueous 60% AcOH Solution

Compound **2** (1 mg) was added to a solution of sinapyl alcohol (**3**, 30 mg, 0.15 mmol) in an aqueous 60% AcOH solution (0.2 mL), followed by an 18 mM aqueous H_2O_2 solution (2 μL, 0.037 mmol), and the resulting reaction solution was kept at room temperature for 7 min. The mixture was then diluted with EtOAc before being washed sequentially with distilled water, a saturated aqueous $NaHCO_3$ solution, and brine. The solution was then dried over anhydrous Na_2SO_4 and concentrated *in vacuo* to give the crude product, which was purified by preparative TLC using a mixture of 3:2 (v/v) of EtOAc and n-hexane to

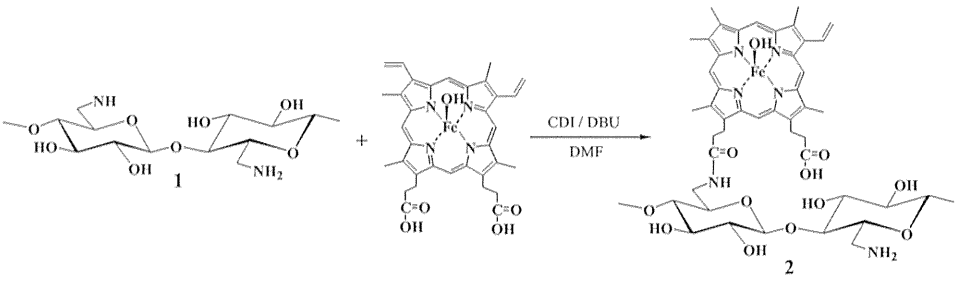

Figure 1. Preparation of hematin-appended 6-amino-6-deoxycellulose (6-ADC/Hem) (**2**).

give (±)-syringaresinol (**4**, 24.8 mg). The synthetic (±)-syringaresinol was then subjected to HPLC analysis.

Results and Discussion

Preparation of Hematin-Appended 6-Amino-6-Deoxycellulose (6-ADC/Hem)(2)

The reaction involving the addition of hematin to 6-amino-6-deoxycellulose (**1**) in the presence of CDI and DBU in DMF at 50°C over four days was ultimately carried out in a heterogeneous system to afford 6-ADC/Hem (**2**) (Figure 1), because our initial attempts to conduct the reaction in a homogeneous reaction system with LiCl and dimethylacetamide were limited by difficulties associated with the purification of compound **2** from the reaction mixture. Compound **2** was soluble in aqueous AcOH solutions containing 60–90% (v/v) AcOH. Compound **2** was subjected to ^{1}H-NMR, FT-IR, and UV-Vis analyses. The high paramagnetic resonance field of the Fe (III) present in hematin had been reported to restrict the unambiguous assignment of the peaks in the NMR spectrum of related compounds.[8] Indeed, the signals in the ^{1}H-NMR spectrum of compound **2** were very broad (data not shown). Pleasingly, however, the broad signals in the range of 3.0 to 5.0 ppm, which were derived from the 6-aminodeoxycellulose, as well as the small characteristic signals at 7.53, 8.20, and 8.80 ppm, which were assigned to the hydroxy ferriprotoporphyrin (HFePP) groups, were all observed in the NMR spectrum of compound **2**. The FT-IR spectrum of compound **2** revealed characteristic bands at 3356 (OH), 2916 (CH), and 1069 (C-O) cm^{-1} derived from the 6-aminocellulose,[13] as well as bands at 1707 (-COOH), 1571, 1384 (CH_3), 1228 (-C-OH), 937, 839, and 715 cm^{-1} (pyrrole-ring) derived from the HFePP groups (Figure 2).[14] There are two possibilities for the linkage between hematin and compound **1**: amide linkage and ester linkage. The model reaction of hematin with D-glucosamine was performed by the modified method for compound **2** to give a model compound (hematin-di-glucosamine) (Figure 3) in 85% yield. The band at 1649 cm^{-1} assignable to amide groups[4] clearly appeared in the FT-IR spectrum of the model compound (Figure 2). These results showed that amino groups of D-glucosamine reacted with hematin preferentially in the presence of hydroxyl groups. Furthermore, a shoulder peak was observed at 1648 cm^{-1} that was assigned to amide groups in the FT-IR spectrum of compound **2** (Figure 2). These results suggested that hematin may be bonded to compound **1** through amide linkages, although further investigation for the confirming of amide linkages was required. The UV-vis spectrum of compound **2** in an aqueous 80% AcOH solution revealed a characteristic band at 398 nm, which is known as the Soret band, as well as satellite bands at 627 and 502 nm, which were derived from the Q bands (Figure 4). These spectroscopic data clearly

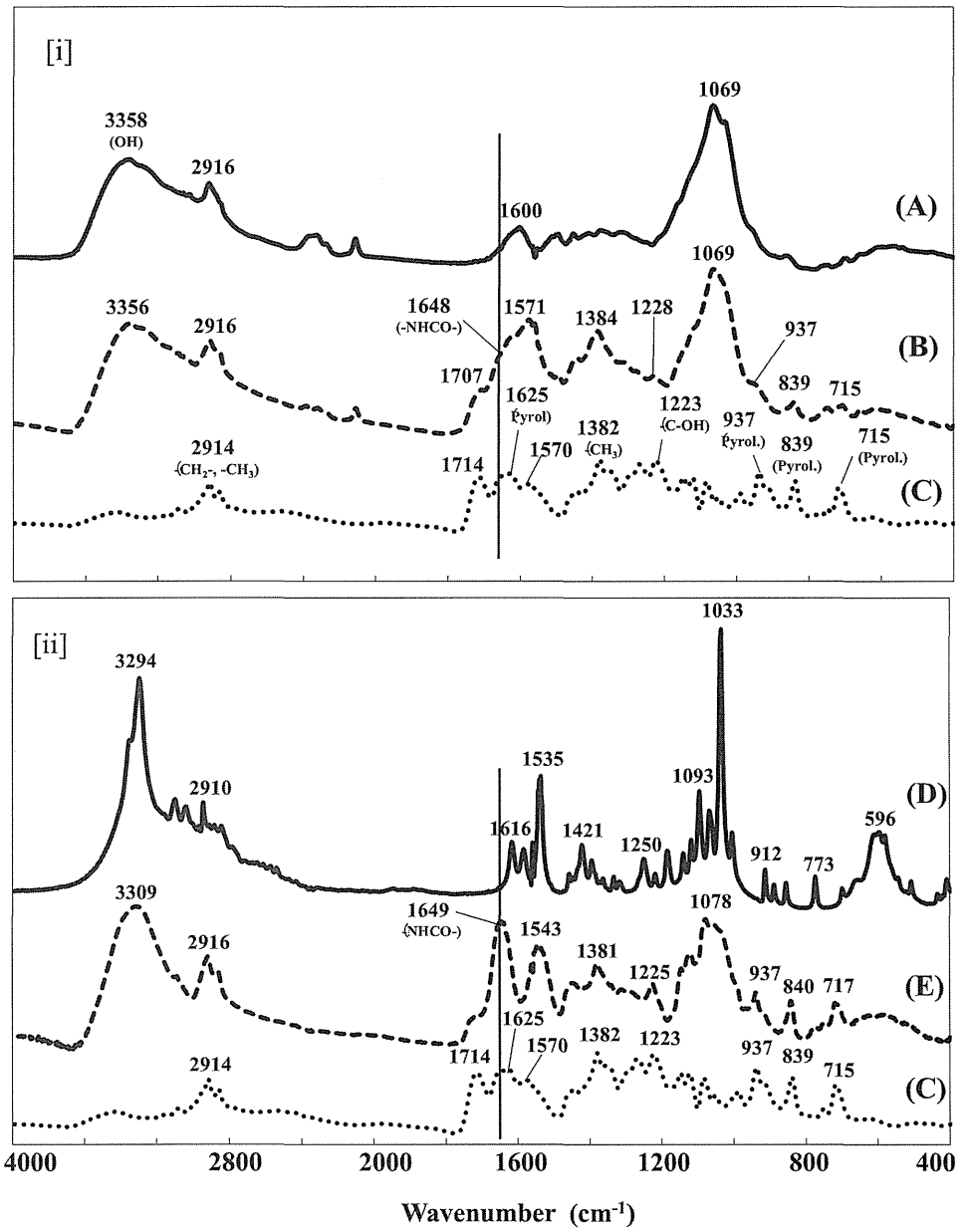

Figure 2. FT-IR spectra of compound **1** (A); 6-ADC/Hem (2) (B); Hematin (C); glucosamine hydrochloride (D); Hematin-di-glucosamine (E).

demonstrated that compound **2** was the expected HFePP-bearing cellulose derivative. The value for the average degree of substitution of the HFePP groups (DS_{HFePP}) in compound **2** was roughly estimated using a UV-vis spectroscopic method (UV detection: 398 nm) with the calibration curves from hematin, although the distribution of HFePP groups was generally believed to be remarkably heterogeneous. The value was found to be 0.11. Another preliminary experiment revealed that the DS_{HFePP} value of compound **2** increased initially

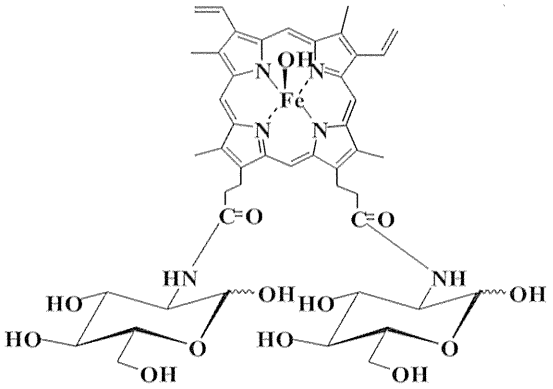

Figure 3. Model compound (Hematin-di-glucosamine).

with increasing reaction time, and then leveled off following three days under the standard reaction conditions described above.

Stability Testing of 6-ADC/Hem (2) in an Aqueous 80% AcOH Solution

Two solutions of compound **2** in an aqueous 80% AcOH solution (pH 1.5) were prepared to evaluate the stability of the HFePP groups of compound **2** under acidic conditions at different temperatures. Thus, one solution was kept at ambient temperature for three days, whereas the other solution was kept at 100°C for 3 h. The maximum absorbance values for the Soret bands (absorbance at 398 nm (A_{398}) for compound **2**, absorbance at 399 nm (A_{399}) for hematin) of the solutions have been listed in Table 1. The A_{398} value of the

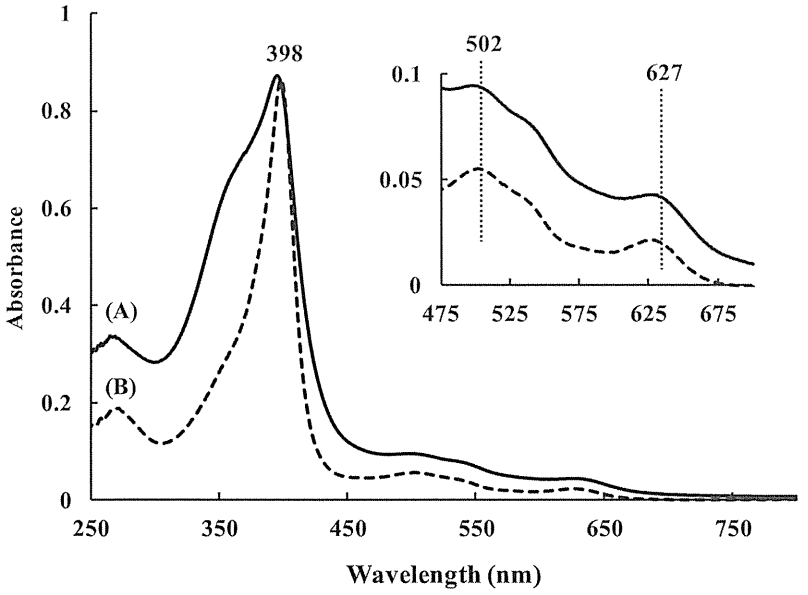

Figure 4. UV-vis spectra of 6-ADC/Hem (**2**) (A); and Hematin (B).

Table 1
Changing of maximum absorbance of 6-ADC/Hem (**2**) and hematin in an aqueous 80% AcOH solution

	Initial	After 3days at r.t.	After 3 h at 100 °C
6-ADC/Hem (**2**)	0.496	0.490	0.478
(398 nm)	(100)	(98.8)	(96.3)
Hematin	0.497	0.399	0.327
(399 nm)	(100)	(80.3)	(65.7)

The data in parentheses are percenatage of maximum absorbance based on the initial absorbance

compound **2** solution was practically unchanged by either of the treatments, whereas the A_{399} value of the hematin solution had been reduced, indicating that the cellulose backbone attributed to the stability of the HFePP groups in an aqueous 80% AcOH solution. The CV measurements of compound **2** and hematin in 5 mM sodium acetate in an aqueous 80% AcOH solution were performed (Figure 5). The first oxidation peaks of compound **2** and hematin were found at 0.92 V and 0.81 V, respectively, but the corresponding reduction peaks were not found, although the CV of the electrolyte seemed to contribute to the CV of compound **2** considerably. Higher oxidation potential of compound **2** might be one of the reasons for the stability of HFePP groups of compound **2**.

Compared with HRP, hematin is known to be highly resistant to a range of different H_2O_2 concentrations in the polymerization of phenol.[15] With this in mind, the stability of the compound **2** solution in the system in the absence of a substrate but in the presence of H_2O_2 (0.9 μmol) was investigated (Figure 6). The A_{398} value of the compound **2** solution decreased more rapidly than the corresponding A_{399} value of the hematin solution, suggesting that a reaction had occurred between the HFePP groups (or hematin) and the H_2O_2. Similar behavior has been reported for hematin in the absence of a substrate in a buffer solution (pH 7.0) but in the presence of H_2O_2 by Akkara et al.[5] Approximately 30 min after the addition of H_2O_2, guaiacol was added to the compound **2** and hematin solutions. Unfortunately, however, the oxidation products of guaiacol were not detected in either of the solutions, suggesting that compound **2** and hematin had been deactivated by

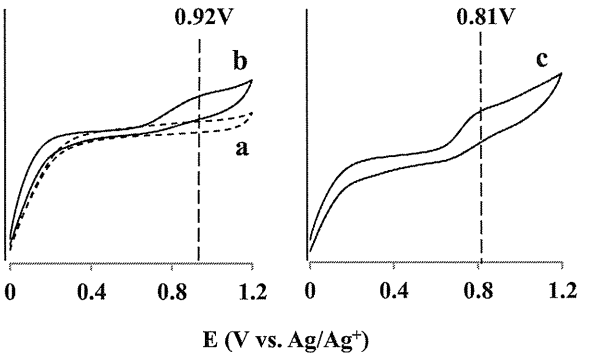

Figure 5. Cyclic voltammograms in an aqueous 80% AcOH solution; background; (a) 6-ADC/Hem (**2**); (b) Hematin; (c) (scan rate: $0.01 Vs^{-1}$).

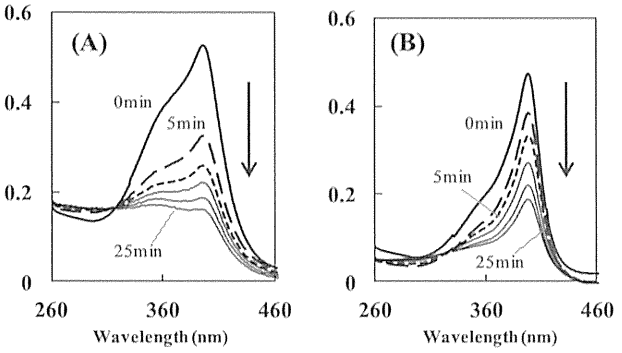

Figure 6. Stability test in the presence of H_2O_2: 6-ADC/Hem (**2**) (A); Hematin (B).

the treatment process. These results revealed that the cellulose backbone did not improve the durability of the HFePP groups towards H_2O_2 in the absence of a substrate.

Guaiacol Oxidation Activity Assay of 6-ADC/Hem (2)

The oxidation of guaiacol is often used as an assay for HRP activity.[16] Figure 5 shows the changes in absorbance at 470 nm (A_{470}) that occurred as a consequence of the guaiacol oxidation products formed during the initial 60 min of the oxidation of guaiacol in an aqueous 80% AcOH solution.

Compound **2** was deactivated in the system described above that did not contain a substrate in the presence of H_2O_2 (0.9 μmol), whereas compound **2** effectively catalyzed the oxidation in the presence of H_2O_2 (9.0 μmol) in the system that contained a substrate (guaiacol). Thus, the A_{470} value increased with increasing reaction time in the case of compound **2**, whereas no discernible changes were observed in the cases of hematin and HRP (Figure 7). These results indicated that compound **2** retained guaiacol oxidation activity even under the strongly acidic conditions, whereas hematin and HRP were deactivated by the conditions. To confirm the stability of compound **2**, the samples were collected after they had been subjected to the treatments described above (i.e., room temperature for three days or 100°C for 3 h) and subjected to the oxidation activity assay. No significant changes were observed in the guaiacol oxidation activity of compound **2** following its treatment at room temperature for three days. Furthermore, the material still provided significant oxidation activity following its treatment at 100°C for 3 h (Figure 7). Based on these results, it is clear that the oxidation activity of compound **2** was retained, as expected from the results of the stability test described above. The rate of the reaction for the compound **2**-catalyzed oxidation at 25°C was found to increase with increasing H_2O_2 concentration (Figure 7).

It was reported that hematin has a propensity to aggregate spontaneously at low pH.[17] One of the reasons for higher oxidation activity and stability of compound **2** might be that the cellulose backbone of compound **2** plays an important role in inhibiting the self-aggregation of the hematin moieties, although further investigation is required.

6-ADC/Hem (2)-Catalyzed Oxidation of Sinapyl Alcohol

It is well known that the oxidative polymerization of sinapyl alcohol (**3**) with HRP preferentially affords the β- β coupling products such as (±)-syringaresinol (**4**), which exists as

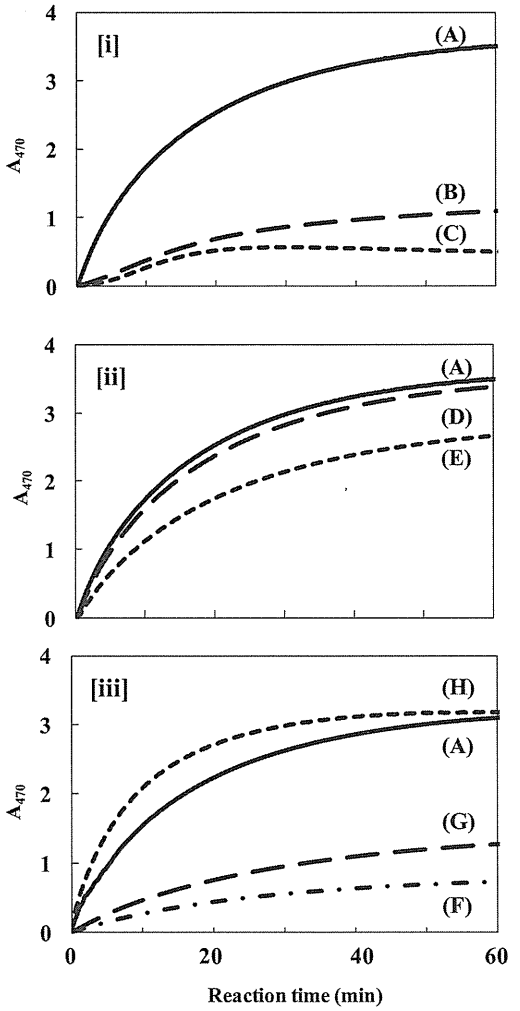

Figure 7. Guaiacol oxidation assay: [i] with H_2O_2 (9 μmol): 6-ADC/Hem (**2**): (A) Hematin; (B) HRP; (C) [ii] with H_2O_2 (9μmol): 6-ADC/Hem (**2**) without treatment; (A) 6-ADC/Hem (**2**) after three days at room temperature; (D) 6-ADC/Hem (**2**) after 3 h at 100°C; (E) [iii] 6-ADC/Hem (**2**) with H_2O_2; 0.9 μmol (F); 1.8 μmol (G); 9 μmol (A); 18 μmol (H).

a racemic mixture.[18] To investigate the influence of the chirality of the cellulose backbone on the reaction, the compound **2**-catalyzed oxidation of sinapyl alcohol (**3**) was performed. An aqueous 60% AcOH solution was selected as a solvent to obtain enough β- β coupling products, because it was found from a preliminary experiment that the yield of a soluble fraction of the product which might be a low-molecular product in the oxidative polymerization in an aqueous 60% AcOH solution was higher than that in the polymerization in an aqueous 80% AcOH solution. As the result, the corresponding dimer products (±)-syringaresinol (**4**) was obtained in 82.6% yield. A HPLC chromatogram of the products is shown in Figure 8. The ratio of (+)-syringaresinol (**4a**) to (-)-syringaresinol (**4b**) was found to be 51.3:48.7, indicating that compound **2** had not provided any asymmetric induction. This lack of asymmetric induction was attributed to the HFePP groups being distributed on

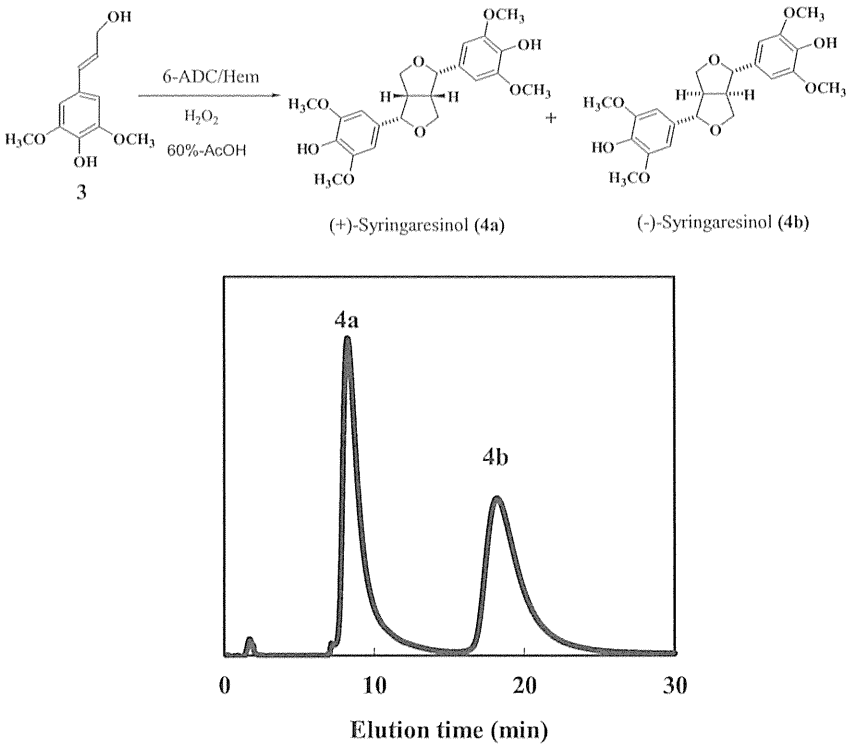

Figure 8. 6-ADC/Hem (**2**)-catalyzed polymerization of sinapyl alcohol (**3**).

compound **2** in a heterogeneous manner together with the general flexibility of compound **2** under the reaction conditions. We are currently investigating further modifications to the structure of compound **2** including, for example, the uniform distribution of HFePP groups and the introduction of other substituents to the C-2 and C-3 hydroxy groups in our laboratory with a view to developing a catalyst capable of asymmetric induction.

Conclusion

We have prepared 6-ADC/Hem (**2**) by the reaction of 6-aminocellulose (**1**) with hematin in the presence of CDI and DBU. Although compound **2** was found to be more stable than hematin under acidic conditions, it was less stable than hematin in the presence of H_2O_2. Compound **2** exhibited good oxidation activity in an aqueous 80% AcOH solution, whereas hematin and HRP were poorly active under these conditions, suggesting that compound **2** would be a useful biomimetic catalyst. Unfortunately, no asymmetric induction was observed in the oxidation of sinapyl alcohol (**3**) with compound **2**.

Funding

This investigation was supported in part by a Grant-in-Aid for Scientific Research from the Ministry of Education, Science and Culture of Japan (No. 20580174).

References

1. Redl, F.X.; Lutz, M.; Daub, J. Chemistry of porphyrin-appended cellulose strands with a helical structure: Spectroscopy, electrochemistry, and in situ circular dichroism spectroelectrochemistry. Chemical European Journal **2001**, *7*, 5350–5358.
2. Dias, S.L.P.; Gushikem, Y.; Ribeiro, E.S.; Benvenutti, E.V. Cobalt(II) hematoporphyrin IX and protoporphyrin IX complexes immobilized on highly dispersed titanium(IV) oxide on a cellulose microfiber surface: Electrochemical properties and dissolved oxygen reduction study. Journal of Electroanalytical Chemistry **2002**, *523*, 64–69.
3. Sakakibara, K.; Ogawa, Y.; Nakatsubo, F. First cellulose Langmuir-Blodgett films towards photocurrent generation systems. Macromolecular Rapid Communications **2007**, *28*, 1270–1275.
4. Boufi, S.; Vilar, M.R.; Parra, V.; Ferraria, A.M.; Botelho do Rego, A.M. Grafting porphyrins on cellulose nanometric films. Langmuir **2008**, *24*, 7309–7315.
5. Akkara, J.A.; Wang, J.; Yang, D.-P.; Gonsalves, K. Hematin-catalyzed polymerization of phenol compounds. Macromolecules **2000**, *33*, 2377–2382.
6. Sakai, S.; Moriyama, K.; Taguchi, K.; Kawakami, K. Hematin is an alternative catalyst to horseradish peroxidase for in situ hydrogenation of polymers with phenolic hydroxyl groups in vivo. Biomacromolecules **2010**, *11*, 2179–2183.
7. Singh, A.; Roy, S.; Samuelson, L.; Bruno, F.; Nakarajan, R.; Kumar, J.; John, V.; Kaplan, D.L. Peroxidase, hematin and peglated-hematin catalyzed vinyl polymerizations in water. Journal of Macromolecular Science – Pure Applied Chemistry **2001**, *A38*(12), 1219–1230.
8. Nagarajan, A.; Nagarajan, R.; Bruno, F.; Samuelson, L.A.; Kumar, J. A stable biomimetic redox catalyst obtained by the enzyme catalyzed amidation of iron porphyrin. Green Chemistry **2009**, *11*, 334–338.
9. Maux, P.L.; Simonneaux, G. First enantioselective iron-porphyrin-catalyzed sulfide oxidation with aqueous hydrogen peroxide. Chem. Commun. **2011**, *47*, 6957–6959.
10. Olsen, K.W. Affinity chromatography of heme-binding proteins: Synthesis and characterization of hematin- and hematoporphyrin-agarose. In: *Methods in Enzymology: Vol. 123, Vitamins and Coenzymes Part H*; Chytil, F.; McCormick, D.B., Eds.; Academic Press: Orlando, FL, USA, 1986, 324–331.
11. Matsui, Y.; Ishikawa J.; Kamitakahara, H.; Takano, T.; Nakatsubo, F. Facile synthesis of 6-amino-6-deoxycellulose. Carbohydrate Research **2005**, *340*, 1403–1406.
12. Yamaguchi, H.; Nakatsubo, F.; Katsura, Y.; Murakami, K. Characterization of (+)- and (-)-syringaresinol di-β-D-glucosides. Holzforschung **1990**, *44*, 381–385.
13. Klemm, D.; Philipp, B.; Heinze, T.; Heinze, U.; Wagenknecht, W. *Comprehensive Cellulose Chemistry*; Wiley-VCH: Weinheim, Germany, 1998.
14. Melki, P.G. Résultats obtenus en spectrographie infrarouge sur quelques porphyrines entre 4000 et 400 cm^{-1}. Biochimie. **1971**, *53*, 875–885.
15. Ambroshio, K.; Rueda, E.; Ferreira, M.L. Magnetite-supported hematin as a biomimetic of horseradish peroxidase in phenol removal by polymerization. Biocatalysis and Biotransformation **2004**, *22*, 35–44.
16. Tonami, H.; Uyama, H.; Nagahata, R.; Kobayashi, S. Guaiacol oxidation products in the enzyme-activity assay reaction by horseradish peroxidase catalysis. Chemistry Letters **2004**, *33*, 796–797.
17. Crespo M.P.; Tilley, L.; Klonis, N. Solution behavior of hematin under acidic conditions and implications for its interactions with chloroquine. J. Biol. Inorg. Chem. **2010**, *15*, 1009–1022.
18. Tanahashi, M.; Higuchi, T. Effect of the hydrophobic regions of hemicelluloses on dehydrogenative polymerization of sinapyl alcohol. Mokuzai Gakkaishi **1990**, *36*, 424–428.

Bioorganic & Medicinal Chemistry 23 (2015) 876–890

Contents lists available at ScienceDirect

Bioorganic & Medicinal Chemistry

journal homepage: www.elsevier.com/locate/bmc

Fused-ring structure of decahydroisoquinolin as a novel scaffold for SARS 3CL protease inhibitors

Yasuhiro Shimamoto [a], Yasunao Hattori [a], Kazuya Kobayashi [a], Kenta Teruya [b], Akira Sanjoh [c], Atsushi Nakagawa [d], Eiki Yamashita [d], Kenichi Akaji [a,*]

[a] Department of Medicinal Chemistry, Kyoto Pharmaceutical University, Yamashina-ku, Kyoto 607-8412, Japan
[b] Department of Chemistry, Graduate School of Medical Science, Kyoto Prefectural University of Medicine, Sakyo-ku, Kyoto 606-0823, Japan
[c] R&D Center, Protein Wave Co., Nara 631-0006, Japan
[d] Institute for Protein Research, Osaka University, Suita, Osaka 565-0871, Japan

ARTICLE INFO

Article history:
Received 8 November 2014
Revised 3 December 2014
Accepted 5 December 2014
Available online 20 December 2014

Keywords:
SARS 3CL protease
Inhibitor
Decahydroisoquinolin
Hydrophobic interaction

ABSTRACT

The design and evaluation of a novel decahydroisoquinolin scaffold as an inhibitor for severe acute respiratory syndrome (SARS) chymotrypsin-like protease ($3CL^{pro}$) are described. Focusing on hydrophobic interactions at the S_2 site, the decahydroisoquinolin scaffold was designed by connecting the P_2 site cyclohexyl group of the substrate-based inhibitor to the main-chain at the α-nitrogen atom of the P_2 position via a methylene linker. Starting from a cyclohexene enantiomer obtained by salt resolution, *trans*-decahydroisoquinolin derivatives were synthesized. All decahydroisoquinolin inhibitors synthesized showed moderate but clear inhibitory activities for SARS $3CL^{pro}$, which confirmed the fused ring structure of the decahydroisoquinolin functions as a novel scaffold for SARS $3CL^{pro}$ inhibitor. X-ray crystallographic analyses of the SARS $3CL^{pro}$ in a complex with the decahydroisoquinolin inhibitor revealed the expected interactions at the S_1 and S_2 sites, as well as additional interactions at the *N*-substituent of the inhibitor.

1. Introduction

Although the primary epidemic of SARS (Severe Acute Respiratory Syndrome)[1–3] affecting about 8500 patients and 800 dead was eventually brought under control, the recent identification of a SARS CoV (coronavirus)-like virus in Chinese bats[4,5] and of a novel coronavirus MERS-CoV (Middle East Respiratory Syndrome Corona Virus, previously known as human CoV-EMC) raise the possibility of a reemergence of SARS or related diseases.[6,7] Since no effective therapy exists for these viral infections, developing anti-SARS agents against future outbreaks remains a formidable challenge.

SARS is a positive-sense, single-stranded RNA virus featuring the largest known viral RNA which produces two large proteins with overlapping sequences, polyproteins 1a (~450 kDa) and 1ab (~750 kDa).[8–10] SARS 3CL (chymotrypsin like) protease ($3CL^{pro}$) is a key enzyme to cleave the polyproteins to yield functional polypeptides.[11,12] The $3CL^{pro}$ is a cysteine protease containing a Cys-His catalytic dyad and it exists as a homodimer; each monomer contains the catalytic dyad at each active site. Due to its functional importance in the viral life cycle, $3CL^{pro}$ is considered an attractive target for the structure-based design of drugs against SARS. Thus, numerous inhibitors of $3CL^{pro}$ have been reported including peptide-mimics[13–17] and small molecules derived from natural products,[18–20] anti-viral agents,[21,22] anti-malaria agents,[23] or high throughput screening.[24–27]

In the course of our own studies on the SARS $3CL^{pro}$ and its inhibitors,[28] we found that the addition of an extra sequence to the N- or C-terminus of the mature SARS $3CL^{pro}$ lowered the catalytic activity and that the mature SARS $3CL^{pro}$ is sensitive to degradation at the 188Arg/189Gln site, which causes a loss of catalytic activity. The stability of $3CL^{pro}$ is dramatically increased by mutating the Arg at the 188 position to Ile. The enzymatic efficiency of the R188I mutant was increased by a factor of more than 1×10^6. The potency of the mutant protease makes it possible to quantitatively evaluate substrate-based peptide-mimetic inhibitors easily by conventional HPLC using a substrate peptide containing no fluorescence derivatives. The evaluations revealed that a peptide aldehyde covering the P-site sequence of substrate, Ac-Ser-Ala-Val-Leu-NHCH($CH_2CH_2CON(CH_3)_2$)–CHO, inhibits the SARS $3CL^{pro}$ with an IC_{50} value of 37 μM. Systematic modification guided by the X-ray crystal structure of a series of peptide-mimics in a complex with R188I SARS $3CL^{pro}$ resulted in **1** with an IC_{50} value of 98 nM (Fig. 1).[13] All of the side-chain structures of **1** differed from the substrate sequence except at the P_3 site, where the side-chain was directed outward. Kinetic inhibition data for **1**

* Corresponding author. Tel./fax: +81 75 595 4635.
E-mail address: akaji@mb.kyoto-phu.ac.jp (K. Akaji).

http://dx.doi.org/10.1016/j.bmc.2014.12.028
0968-0896/

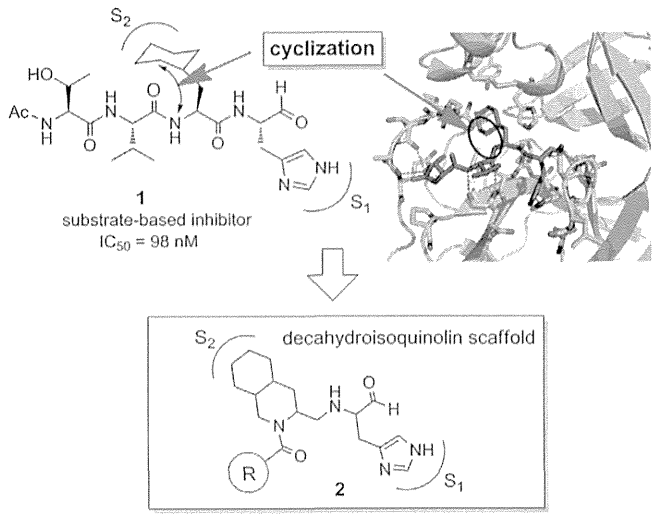

Figure 1. Design of a decahydroisoquinolin scaffold.

obtained from Lineweaver–Burk plots suggested that inhibitors containing an aldehyde at the C-terminus can be expected to function as competitive inhibitors.

In the present study, we designed a novel non-peptide inhibitor focusing on the interactions at the S_1 and S_2 sites of the $3CL^{pro}$ Confirmed to be critical to make the **1** potent competitive inhibitor. Among the key interactions clarified by X-ray crystallographic study, we focused on hydrophobic interactions at the cyclohexyl side-chain to design a novel inhibitor scaffold. Thus, the cyclohexyl ring is connected to the main-chain at an α-nitrogen atom of the P_2 position Cha (cyclohexylalanine) via a methylene linker to yield compound **2** (Fig. 1). The resulting decahydroisoquinolin scaffold of **2** is expected to keep the hydrophobic interactions at the cyclohexyl ring of the substrate-based inhibitor at the S_2 pocket. In addition, the resulting decahydroisoquinolin scaffold arranges the P_1 site imidazole and active site functional aldehyde at each required position, giving the fused-ring structure of decahydroisoquinolin as a scaffold for a novel inhibitor. The acyl substituent on the nitrogen in the decahydroisoquinolin scaffold may add an extra position for the interactions with the $3CL^{pro}$.

2. Results and discussion

2.1. Chemistry

The retro synthetic route for the desired decahydroisoquinolin derivative **2** is shown in Scheme 1. The P_1 site His derivative could be introduced by a reductive amination reaction using an aldehyde derivative prepared by oxidative cleavage of the olefin bond of **3**. The *trans*-decahydroisoquinolin scaffold of **3** could be constructed via Pd-mediated stereoselective intra-molecular cyclization[29] by nucleophilic attack of a nitrogen atom to the Pd-activated olefin moiety of an allyl alcohol of **4**. The olefin structure of **4** could be constructed by a Horner–Emmons reaction utilizing an aldehyde of precursor **5**, and the amino group of **4** could be introduced by a Mitsunobu reaction to the alcohol of **5**. The six-membered ring structure of **5** could be constructed by a Diels–Alder reaction of known ester **6**[30] with butadiene.

Thus, the key intermediates **12** and **13**, a precursor of the Pd-mediated cyclization, were prepared according to the route shown in Scheme 2. The known ester **6** was first reacted with butadiene to construct the six-membered ring structure to yield **7** as an enantiomer mixture of 1,6-*trans*-substituted cyclohexene. The product was reduced with LAH and the resulting alcohol was then protected as *tert*-butyldiphenylsilyl ether to give **8**. The benzyl group was removed by catalytic hydrogenation, which reduced the cyclohexene to cyclohexane at the same time. The resulting hydroxyl group was then oxidized with PCC and the resulting aldehyde was then reacted with $(EtO)_2P(O)CH_2COOEt$ to yield **9**. The ethyl ester of **9** was reduced with DIBALH and the resulting alcohol was protected as acetyl ester to give **10**. After treatment with TBAF, the resulting alcohol was converted to the azide derivative **11** by a Mitsunobu reaction. Since the product **11** was rather unstable, **11** was immediately reduced to the corresponding amine. Without further purification, the amine derivative was coupled with *p*-phenylbenzoic acid using HBTU to yield **12** as an enantiomer mixture. Coupling with *p*-bromobenzoic acid was similarly conducted to yield a related derivative **13**.

Construction of the decahydroisoquinolin scaffold was achieved as shown in Scheme 3. $(CH_3CN)_2PdCl_2$-mediated cyclization of **12/13** gave the desired *trans*-decahydroisoquinolin derivative **14/15** as a major product. The product was an enantiomer mixture which was thought to have the relative configuration of **14/15** due to the cyclization through a less hindered Pd-chelated intermediate. Thus, the vinyl substituent of the product **14/15** was thought to be axial, which was clearly confirmed by X-ray crystallographic studies of the inhibitor in a complex with the R188I mutant SARS $3CL^{pro}$ as discussed below. The olefin bond of **14/15** was oxidatively cleaved by the treatment with $K_2O_5O_2(OH)_4$ followed by $NaIO_4$ to yield aldehyde **16/17**. Reductive amination by H-His(Trt)-N(OCH_3)-CH_3 gave the coupling products **18** and **20** or **19** and **21** as a 1:1 diastereomer mixture which was separable on a reversed-phase column (YMC Pack ODS) by analytical HPLC (Fig. S1). The diastereomers could also be separated by conventional silica-gel column chromatography to yield diastereomers **18** and **20** or **19** and **21**, each having single peak on the above reversed-phase column. Each separated diastereomer was then treated with TFA to cleave the Trt group at the imidazole ring, and the product was reduced with DIBALH to yield the desired aldehyde **22/23** or **24/25**. Although the absolute configuration of each product was not determined at this stage, the purity of each product was confirmed by analytical HPLC. Since moderate but clear inhibitory activities were observed in a preliminary evaluation on the inhibitory potency of **22** and **24**, the identification of the stereo-structure was then conducted.

To separately prepare the above diastereomers and estimate the absolute configurations, cyclohexene carboxylic acid obtained by a Diels–Alder reaction was converted to a salt with (*R*)- or (*S*)-α-methylbenzylamine and resolved according to the literature procedure for (1*R*/6*S*,1*S*/6*R*)-6-(2-bromophenyl)cyclohex-3-ene-1-carboxylic acid **26**[31] (Scheme 4). Resolution of a carboxylic acid derived from compound **7** and compound **29** having the corresponding *p*-bromobenzyl group gave compounds showing the same polarimetric characters as the literature compounds.[31] (−) Carboxylic acid **27** or **30** was obtained by salt formation with (*R*)-α-methylbenzylamine and following salt-liberation with HCl, whereas the salt with (*S*)-α-methylbenzylamine gave (+) carboxylic acid **28** or **31**. Compared with the literature values, these results strongly suggest that **27** and **30** would have (1*R*,6*S*) and **28** and **31** would have (1*S*,6*R*) absolute configurations. Optical purity of each enantiomer was further confirmed using a chiral column (YMC CHIRAL Amylose-C) by HPLC (Fig. S2). Since the chemical yield from the *p*-bromobenzyl derivative **29** was superior to the benzyl derivative **7**, enantiomer **30** or **31** was used as the starting compound for the separate synthesis of decahydroisoquinolin diastereomers.

The separated (1*S*,6*R*) enantiomer **31** was then used to synthesize the corresponding decahydroisoquinolin diastereomer **40** or **41** using basically the same route as above (Scheme 5i). (1*R*,6*S*) Enantiomer **30** was also employed for the syntheses of diastereo-

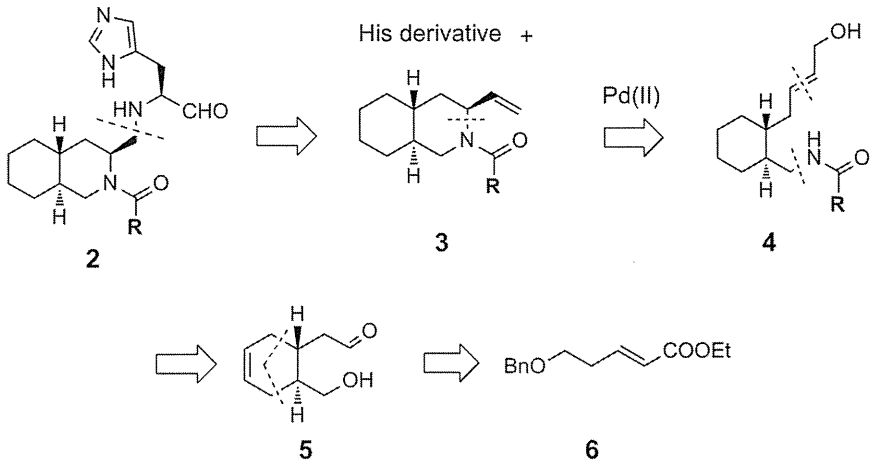

Scheme 1. Retro synthetic route for the decahydroisoquinolin derivative.

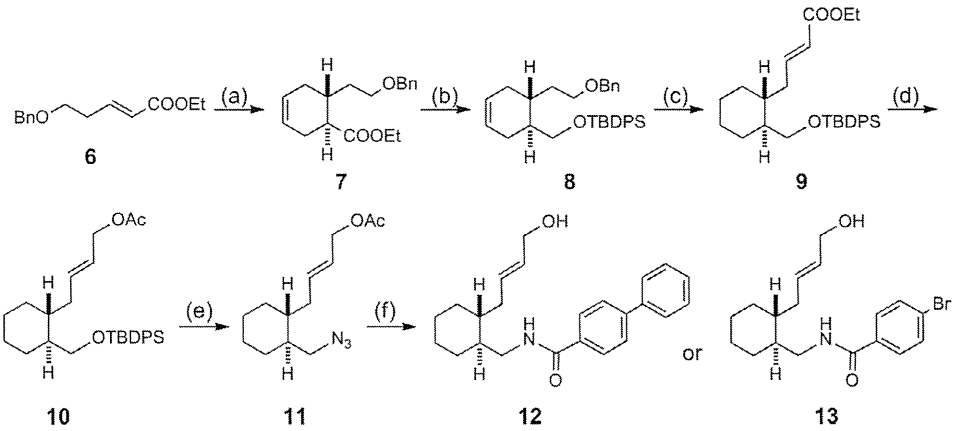

Scheme 2. Synthesis of intermediate **12** or **13**. Configurations in the racemic compounds **7–13** indicate the relative 1,6-*trans* configurations. Reagents: (a) 1,3-butadiene; (b) (1) LAH, (2) TBDPS-Cl/imidazole; (c) (1) H_2/Pd(OH)$_2$-C (2) PCC (3) $(EtO)_2P(O)CH_2COOEt$/NaH; (d) (1) DIBALH (2) Ac_2O/pyridine/DMAP; (e) (1) TBAF, (2) $(EtO)_2P(O)N_3$/DIAD/PPh_3; (f) (1) LAH, (2) 4-phenylbenzoic acid or 4-bromobenzoic acid/HBTU/DIPEA.

mer **44** or **45** (Scheme 5ii). The protected intermediate **38** (R = *p*-phenylphenyl) from **31** and the diastereomer **42** (R = *p*-phenylphenyl) from (1*R*,6*S*) enantiomer **30** were co-eluted with a previously synthesized diastereomixture of **18** and **20** on a reversed-phase column (YMC Pack ODS). Intermediate **38** had the same retention time as **18**, whereas intermediate **42** had the same retention time as **20** (Fig. S3). The comparison was also conducted on **39** and **43** having a *p*-bromophenyl *N*-substituent with the corresponding diastereomers **19** and **21**, and the same results as above were obtained (Fig. S4). These results clearly demonstrated that the two diastereomers **18** and **20** were derived from the *trans*-decahydroisoquinolin structure constructed from enantiomer **7**. Each protected diastereomer **38/39** and **42/43** thus synthesized was converted to the desired derivatives **40/41** and **44/45** without difficulty. Several analogs shown in Table 1 containing different *N*-acyl substituents of the decahydroisoquinolin scaffold were also prepared using the same synthetic route (Fig. S5).

2.2. Inhibitory activity

Digestion of the substrate peptide with R188I SARS 3CL^{pro} in the presence of decahydroisoquinolin derivatives of different concentrations was conducted according to the published procedure.[13] The inhibitory activities were evaluated based on IC_{50} values calculated from the decrease in the substrate digested by R188I SARS 3CL^{pro}; a typical sigmoidal curve used for estimation of the IC_{50} value is shown in Figure S6. As summarized in Table 1, synthesized decahydroisoquinolin derivatives all showed inhibitory activities for the mutant 3CL^{pro}. The results strongly suggest that the decahydroisoquinolin fused-ring can function as an inhibitor scaffold. Comparison of IC_{50} values of *trans*-decahydroisoquinolin diastereomers in *N*-4-phenylbenzoyl derivatives (**40** vs **44**) or *N*-4-bromobenzoyl derivative (**41** vs **45**) clearly showed that the (4a*R*,8a*S*) isomer is more potent than (4a*S*,8a*R*) isomer. The results suggest the importance of the interaction at the S_2 pocket of the mutant 3CL^{pro}. It was also demonstrated that a series of the *N*-benzoyl derivative was more potent than *N*-4-phenylbenzoyl derivatives. Substitution at the 4-position of the benzoyl substituent in **48** with halogen showed no significant effect on the inhibitory activity (**41** and **49**), whereas substitution at the 4-position of the phenyl group in the *N*-biphenylacyl derivative **40** gave a slightly more potent inhibitor than 2- or 3-substituted biphenyl derivatives (**46** and **47**). The results suggest that the substituent on the nitrogen atom of the decahydroisoquinolin scaffold may have some interactions with R188I SARS 3CL^{pro}.

2.3. Evaluation of the interactions

To clarify the interactions of a newly synthesized decahydroisoquinolin inhibitor with R188I SARS 3CL^{pro}, the structure of

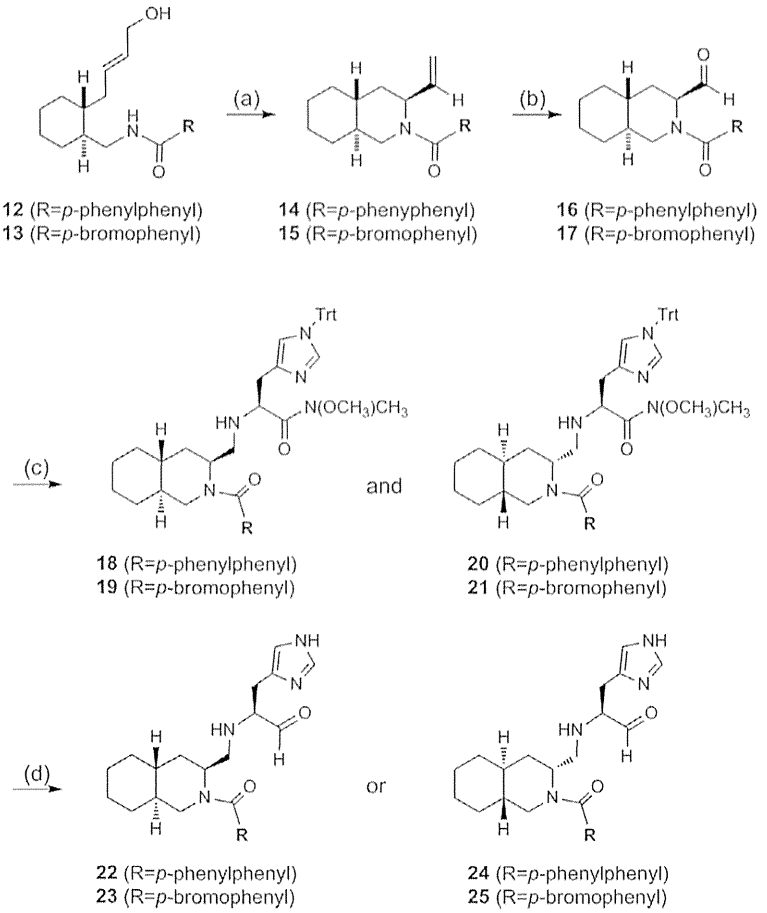

Scheme 3. Construction of the decahydroisoquinolin scaffold. Reagents: (a) $(CH_3CN)_2PdCl_2$; (b) $K_2OsO_2(OH)_4/NaIO_4$; (c) (1) H-His(Trt)-$N(OCH_3)CH_3/NaBH_3CN$; (d) (1) TFA, (2) DIBALH.

the protease in a complex with the inhibitor was revealed by X-ray crystallography. Subsequently, a co-crystal of the inhibitor with $3CL^{pro}$ was prepared and analyzed. Structures of the $3CL^{pro}$ in a complex with inhibitors **40**, **41**, and **44** were refined to resolutions of 1.60 Å, 2.42 Å, and 1.89 Å, respectively (PDB code 4TWY, 4TWW, and 4WY3). The data obtained are summarized in Table 2.

The overall structure of the $3CL^{pro}$ in complex with inhibitor **41** (IC_{50} = 63 μM) was first compared with the substrate-based inhibitor **1** (PDB code 3ATW) (Fig. 2). Basically, the decahydroisoquinolin inhibitor **41** was at the active site cleft of the $3CL^{pro}$ as observed in the highly potent inhibitor **1**. The aldehyde group and imidazole ring of His-al, as well as the decahydroisoquinolin structure of **41**, had an almost identical conformation with **1** and similarly interacted with $3CL^{pro}$. In contrast, the direction of the *p*-bromobenzoyl group was outward from $3CL^{pro}$ and opposite to the P_3 to P_4 sites of **1**. The *N*-*p*-bromobenzoyl group, however, was at the surface of $3CL^{pro}$, where additional hydrophobic interaction with Met of the $3CL^{pro}$ may be possible (Fig. S7).

The carbonyl carbon of the aldehyde group in **41** was detected at a distance of 2.43 Å from the active center thiol of Cys-145, and its electron density could be fitted to an sp^2 carbonyl carbon as in **1** (Fig. 3i). The results suggest that the decahydroisoquinolin inhibitor would function as a competitive inhibitor as do the peptide-aldehyde inhibitor **1**.[13] It was clearly confirmed that the decahydroisoquinolin scaffold of **41** took a *trans*-fused (4a*R*,8a*S*) configuration, as expected from the salt-resolution of enantiomixture **29**. It was also confirmed that the P_1 His-al substituent on the decahydroisoquinolin scaffold took an axial-configuration, as expected from the Pd(II)-mediated cyclization. The decahydroisoquinolin scaffold of **41** was inserted into a large S_2 pocket created by His-41, Met-49, Met-165, and Asp-187, as in the case of a parent peptide aldehyde inhibitor, and most of the S_2 pocket was occupied by the fused-ring structure of decahydroisoquinolin (Fig. 3i). The nitrogen atom of the P_1 site imidazole of **41** formed a hydrogen bond with the imidazole nitrogen of His-163, resulting in close fitting at the other side of the S_1 pocket formed from the Phe-140, Leu-141, and Glu-166 side chains of the protease (Fig. 3ii). These interactions, especially of the decahydroisoquinolin scaffold in the S_2 pocket, function to hold the P_1 site imidazole and terminal aldehyde tightly inside the active site cleft, which resulted in the compact fitting of the novel scaffold to the $3CL^{pro}$.

To evaluate the effects of absolute configuration of the decahydroisoquinolin scaffold, structures of the $3CL^{pro}$ in complex with (4a*R*,8a*S*)-*N*-4-phenylbenzoyl decahydroisoquinolin inhibitor **40** and (4a*S*,8a*R*)-*N*-4-phenylbenzoyl decahydroisoquinolin inhibitor **44** were compared (Fig. 4i). In both inhibitors, the P_1 site imidazole ring and the terminal aldehyde group had nearly the same interactions as in the (4a*R*,8a*S*)-*N*-bromobenzoyl decahydroisoquinolin inhibitor **41** described above. Due to the configuration change at the decahydroisoquinolin moiety, however, the (4a*S*,8a*R*) decahydroisoquinolin scaffold was clearly twisted compared to the (4a*R*,8a*S*) decahydroisoquinolin in the S_2 pocket (Fig. 4ii). This conformation change of the decahydroisoquinolin scaffold transferred to the direction of the *N*-substituent. Thus, the substituent of (4a*R*,8a*S*) decahydroisoquinolin **40** took nearly the same conformation as the *N*-*p*-bromobenzoyl inhibitor **41** located on the surface of the $3CL^{pro}$, whereas the substituent of (4a*S*,8a*R*) decahydroisoquinolin directed outside from the protease surface. These